Electronic Supplementary Material (ESI) for Sustainable Energy & Fuels.

Supporting Information for:

Spontaneous Mesostructure Formation Produces Optically Transmissive NiP Films That are Catalytically Active for the Photoelectrochemical Hydrogen Evolution Reaction

Zachary P. Ifkovits,[1] Jillian T. Reed, [1] Paul A. Kempler,[1] Madeline C. Meier,[1] Sean T. Byrne,[1] Shaoyang Lin,[1] Alexandre Z. Ye,[1] Azhar I. Carim,[1,2] and Nathan S. Lewis[1,2*]

[1]Division of Chemistry and Chemical Engineering, California Institute of Technology, Pasadena, California 91125, USA.

[2]Beckman Institute Molecular Materials Resource Center, California Institute of Technology, Pasadena, California 91125, USA.

[*]Corresponding author: nslewis@caltech.edu

Experimental Details

Materials:

Copper sheets (Cu, 99.999%, Alfa Aesar), indium-gallium eutectic (In-Ga, 99.99%, Alfa Aesar), sodium hypophosphite monohydrate ($NaPO_2H_2 \cdot H_2O$, Sigma), nickel chloride ($NiCl_2$, 98%, Sigma), boric acid (H_3BO_3, >99.5%, Sigma), and sodium chloride (NaCl, 99%, Macron Chemicals) were commercially available and used as received. Sulfuric acid (H_2SO_4, TraceMetal grade, Thermo Fisher Scientific), and hypophosphorous acid (H_3PO_2, 50% weight in water, VWR International) were diluted with deionized water with a resistivity of >18.2 MΩ·cm produced by a Barnstead Nanopure system. 100 mm diameter, 525 μm thick n^+-type (100)-oriented Si wafers with a nominal resistivity of < 0.005 Ω·cm, and p-type (100)-oriented Si wafers of the same dimensions with a nominal resistivity of 1-10 Ω·cm, were purchased from Addison Engineering.

Working Electrode Fabrication:

15-30 mm^2 chips of n^+-Si or doped homojunction n^+-p-Si were used as the substrates for working electrodes. To promote adhesion between the substrates and the electrochemically deposited layer, metallic Ti and then Ni were each sputtered (AJA Orion) onto the samples for 90 s at deposition powers of 130 W and 100 W, respectively, Ohmic contacts were formed by scratching In-Ga eutectic into the backside of the chips with a scribe. Insulated Sn-coated Cu wires with stripped ends were fed through a 6 mm borosilicate glass tube. The wire was sealed into the glass tube using epoxy (Hysol 9460). Samples were attached to the wire with Ag paint that had a grain size < 1.0 μm (PELCO, Ted Pella), and the back of the electrode was sealed using clear nail polish (Sally Hansen). After the film had been deposited, the sealant was readily removed with a razor blade and the sample was separated from the wire. To prepare electrodes with Cu substrates, a Cu sheet was hand polished using a circular motion for 5 min for each different grit size: 2400 (European FEPA standard), followed by 3000, and then by 4000. This sheet was cut with scissors into smaller 10-20 mm^2 pieces. The Cu substrates were attached to an electrode assembly by the same process as described above for Si substrates, but without the In-Ga contact.

Film Deposition:

Shortly before film deposition, metalized n^+-Si samples were sprayed with deionized H_2O and dried under a stream of N_2(g). The Cu substrates were etched for 60 s in 6.6 M HCl(aq) to

remove surface oxides. Electrodeposition of the NiP film was performed in a single-compartment borosilicate glass cell that contained 0.15 M H_3BO_3, 0.10 M NaCl, 0.30 M $H_2NaPO_2 \cdot H_2O$, and 0.20 M $NiCl_2$. The pH of the solution was adjusted from 6.5 to 3.5 by dropwise addition of H_3PO_2(aq) (10% wt). Control over either the current or potential of the working electrode was obtained using a Biologic SP-200 potentiostat. The electrolyte was purged with N_2(g) for at least 30 min prior to the deposition and the flow of N_2 (g) was maintained during the deposition process. A saturated calomel electrode (SCE) was used as the reference electrode, and a Ni foil electrode was used as the counter electrode.

A thermocouple was immersed directly into the electrolyte to monitor the deposition temperature. The cell was secured to a ring stand with a clamp and held in a water bath so that the water completely surrounded the solution without contaminating the cell. A hot plate was used to raise the temperature of the water bath above room temperature (20 ºC). A magnetic stir bar was placed inside the cell and stirring at a rate of 280 RPM was performed for the duration of the deposition. Depositions onto n^+-Si and Cu were performed at a current density of -20 mA cm^{-2}. Electrodepositions onto the photoactive n^+-p-Si/Ti/Ni electrodes were performed using a light-emitting diode (LED) source that had an intensity-weighted average wavelength of 630 nm and approximate intensity of 600 mW cm^{-2}. In these photoelectrochemical depositions, the working electrode was held potentiostatically at -0.6 V vs. SCE.

Electrochemical Measurements and Physical Characterization

The catalytic behavior of the Ni-P films for the hydrogen-evolution reaction was measured at ambient temperature in 0.50 M H_2SO_4(aq) that was purged with H_2(g). A saturated calomel electrode (SCE) was used as the reference electrode, and a graphite rod was used as the counter electrode. Measurements were obtained using a Biologic SP-200 potentiostat. Photoelectrochemical hydrogen evolution experiments were performed in H_2-purged 0.50 M H_2SO_4(aq) under the equivalent of 100 mW cm^{-2} of solar Air Mass 1.5 illumination produced by a calibrated Xe lamp.

Scanning-electron micrographs (SEMs) were recorded with a FEI Nova NanoSEM 450 at an accelerating voltage of X kV with a working distance of 5 mm and in-lens secondary electron detector. Energy-dispersive X-ray (EDX) spectroscopy was performed in the SEM to determine the bulk composition of the NiP films. An accelerating voltage of 10 kV and an Oxford Instruments

X-Max Si drift detector was utilized. Spectra were collected in the range of 0 to 10 keV and quantitative film compositions were derived from these spectra using the "Inca" software package (Oxford Instruments). All other observed elements were either attributable to the electrode base (Ti, Si, or Cu) or were negligible in intensity.

X-ray photoelectron spectroscopy (XPS) was performed using a Surface Science M-Probe ESCA/XPS. The chamber base pressure was $< 2 \times 10^{-8}$. The X-ray source was a monochromatic Al Kα source. The data were analyzed using CasaXPS computer software. A Shirley background was used for all spectra, which were referenced to adventitious C at a binding energy of 284.8 eV.

Atomic force microscopy was performed using a Bruker Dimension Icon to image the surface morphology of the deposited films. The instrument was operated in ScanAsyst mode using a silicon nitride probe (ScanAsyst-Air). The data were collected using scan areas of 500 nm x 500 nm with a probe velocity 500 nm s^{-1} and a pixel size of 1.95 nm x 1.95 nm. Raw data were corrected for sample tilt using the Bruker NanoScope Analysis software.

Samples of NiP films electrodeposited onto FTO/Ti/Ni substrates were analyzed using a Cary 5000 UV-vis-NIR with an integrating sphere. Optical transmission measurements were performed after subsequent etching cycles of the same samples at open circuit in 0.50 M H_2SO_4(aq).

Samples of NiP films electrodeposited onto n^+Si/Ti/Ni substrates were removed from the electrode body by use of a razor blade. The nail polish used to seal the back-contact of the electrode was rigorously removed with the razor blade and isopropyl alcohol, when necessary. The sample chips were then placed in screw cap septum vials (2 mL) and submerged in a mineral oil bath. The bath was stepped from ambient temperature to 200 °C in 25 °C increments. The data shown in Figure 3 were collected after samples had been held for 10 min at 200 °C. For each measurement, 0.2 mL of the headspace was injected into an Agilent 7890A gas chromatography system equipped with a thermal conductivity detector (TCD), Ar as the carrier gas, a backflush system with a PoraPLOT Q column as the pre-column, and a HP-PLOT Molesieve column as the main column. The quantity of the hydrogen was calculated based on a calibration curve.

The optical properties of the NiP samples were characterized using a spectroscopic ellipsometer with a rotating analyzer (J.A. Woolam Co., Inc.). Data were recorded from 300 to 1100 nm in 10 nm increments at an angle of incidence of 70º. The refractive index (n) and

extinction coefficient (k) of the film were determined using a Maxwell-Garnett effective medium approximation.

Supporting Figures

Cross-Sectional SEMs

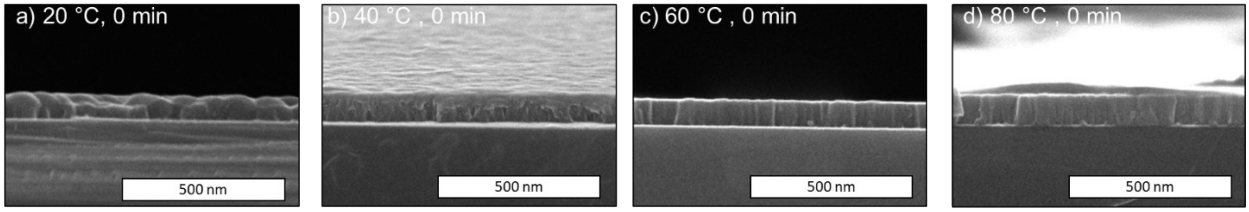

Figure S1. Cross-sectional SEMs of as-deposited NiP films with a cathodic charge density passed of 400 mC cm^{-2} in electrodeposition baths at (a) 20 °C, (b) 40 °C, (c) 60 °C, and (d) 80 °C.

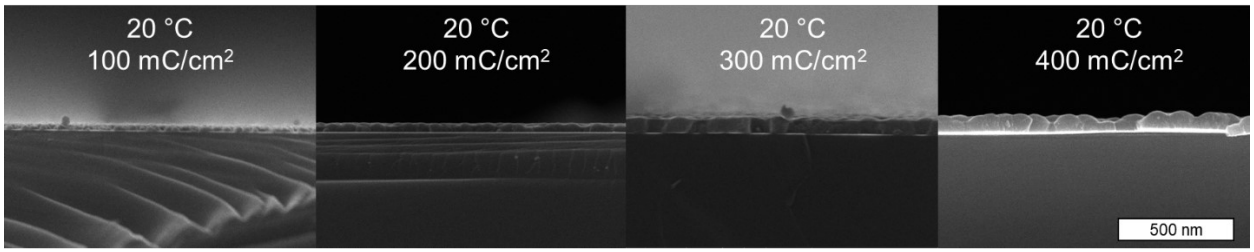

Figure S2. Cross-sectional SEMs of as-deposited Ni-P films at 20 °C, for a range of cathodic charge density passed between 100-400 mC cm^{-2}.

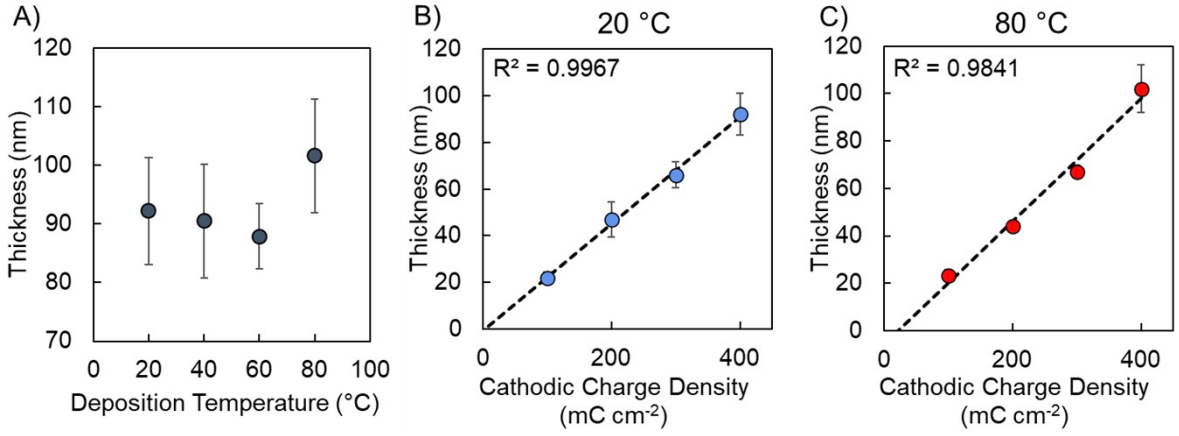

Figure S3. Thickness of deposited films as determined from cross-sectional SEMs in (a) Figure S1 for films deposited at 400 mC cm^{-2} (b) from Figure S2 of films deposited at 20 °C over a range of cathodic charge density, and (c) of films deposited at 80 °C over a range of cathodic charge density.

Cross-sectional SEMs used to determine the thickness of electrodeposited films were based on $n > 7$ measurements from multiple spots along duplicate samples. The Ni-P film thickness was determined to be ~90-100 nm at all temperatures, when 400 mC cm^{-2} of charge density was passed during electrodeposition (Figure S3a). The measured film thicknesses deposited at 20 °C and 80 °C increased linearly as a function of the charge density passed (Figure S3b-c). A linear fit showed the growth rates to be 0.23 nm cm^2 mC^{-1} and 0.26 nm cm^2 mC^{-1} for the $NiP_{20°C}$ and $NiP_{80°C}$ films, respectively. Forcing the line in S3c through the origin reduces the rate to 0.24 nm cm^2 mC^{-1}, and a straight line fit through the origin to the point at 400 mC cm^{-2} changes the rate to 0.255 nm cm^2 mC^{-1}. Measurements for the $NiP_{20°C}$ films were taken across the top of the film, so the reported deposition rate is likely an overestimation as those films were not as conformal in cross-section as films deposited at higher temperatures.

Photos of Working Electrodes during Electrodeposition

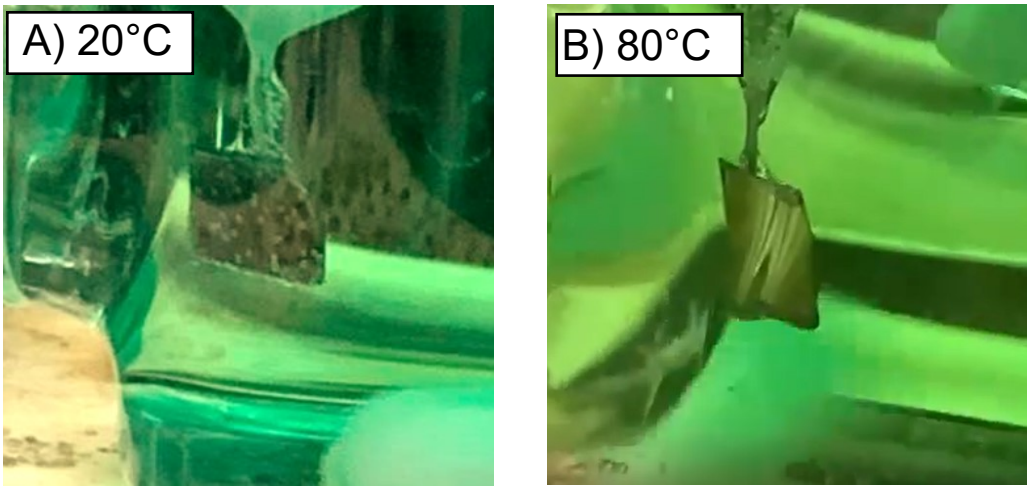

Figure S4. Still frames taken from videos of electrodeposition of NiP at -20 mA cm^{-2} onto n^+Si/Ti/Ni electrodes in NiP deposition baths at A) 20 °C and B) 80 °C.

Figure S4a shows the presence of $H_2(g)$ bubbles across the entire surface of the n^+Si/Ti/Ni working electrode while the electrode was passing -20 mA cm^{-2} in a deposition bath at 20 °C. Figure S4b shows the surface of an identical electrode at -20 mA cm^{-2} in a deposition bath at 80 °C. The slight yellow hue in Figure S4b is due to the yellow/beige-colored top surface of the hot plate that was used to heat the deposition solution.

Faradaic Efficiency Measurements

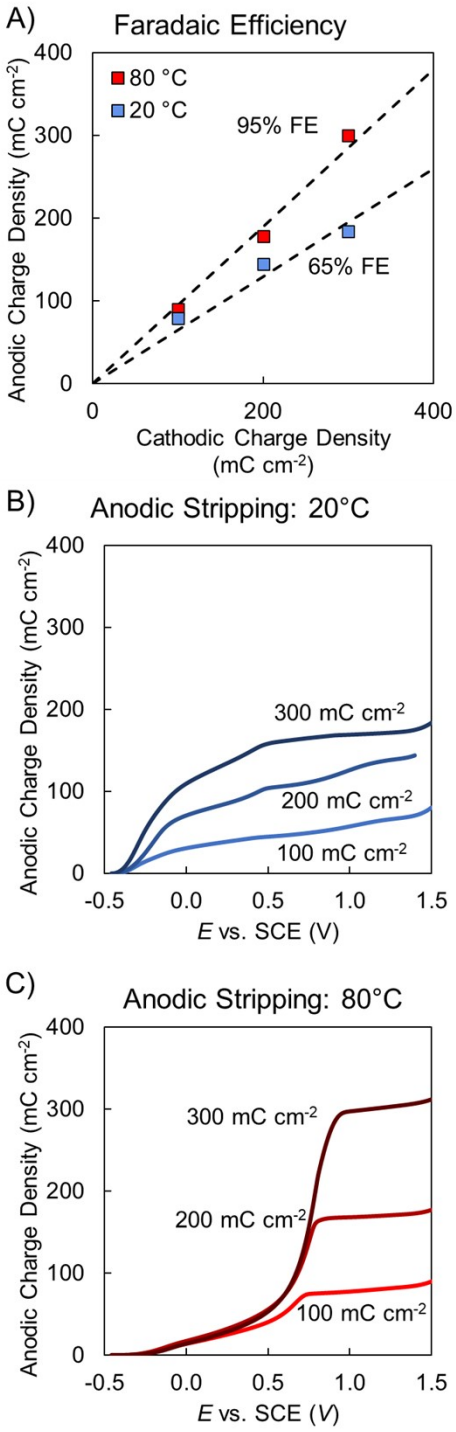

Figure S5. (a) Summary of anodic stripping measurements demonstrating the faradaic efficiency of Ni-P electrodepositions at 20°C (blue) and 80°C (red), as well as dashed lines showing expected values at 65% and 95% faradaic efficiency, (b) net anodic charge density passed under a linear sweep of potential for films deposited at 20°C, (c) net anodic charge density passed under a linear sweep of potential for films deposited at 80°C.

EDX compositional data

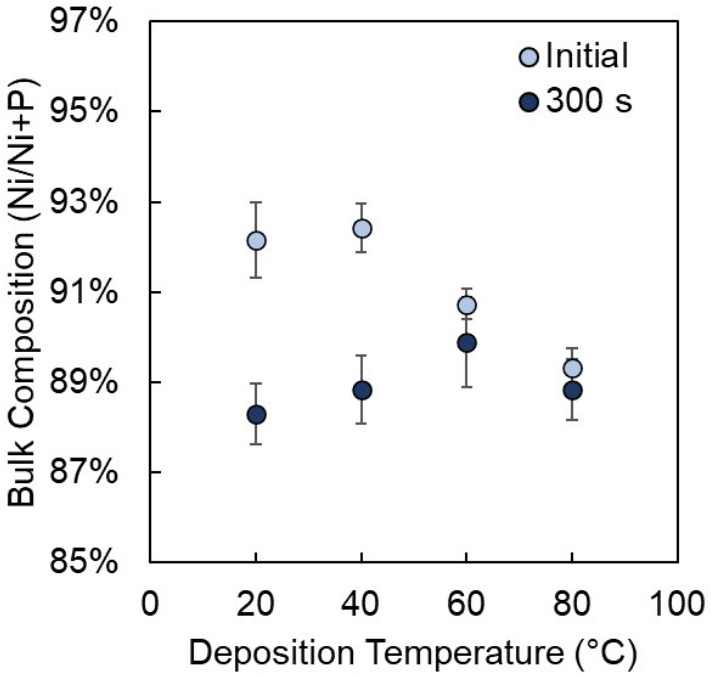

Figure S6. Nickel composition of deposited Ni-P films before (light blue circle) and after (dark blue circle) etching for 300 s in 0.50 M H_2SO_4(aq) as determined by EDX from ≥ 12 regions of replicate samples.

The long-term stability of these photocathodes was not assessed as the Ni-P is electrodeposited directly onto an unprotected silicon surface, which is susceptible to chemical oxidation and degradation in acidic electrolytes, but the photoelectrodes showed stability for as long as they were analyzed (~30 minutes to 1 hour). The catalytic films deposited onto metallic substrates showed stable operation for hours (Figure 4b). We did not determine the behavior of films deposited at temperatures below room temperature, but we do not believe this experiment is necessary to support our conclusions.

Table S1. Summary of top-down and cross-sectional EDX measurements of $NiP_{20°C}$ films

Sample	Collection Angle	Depth from Surface (nm)	Ni Composition (Ni/Ni+P)
As deposited	Top-Down	N/A	92.1% ± 0.8%
As deposited	Cross section	~10 nm	90.6% ± 0.6%
As deposited	Cross section	~50 nm	91.3% ± 0.6%
As deposited	Cross section	~90 nm	90.6% ± 2.3%

XPS Oxidation State Data

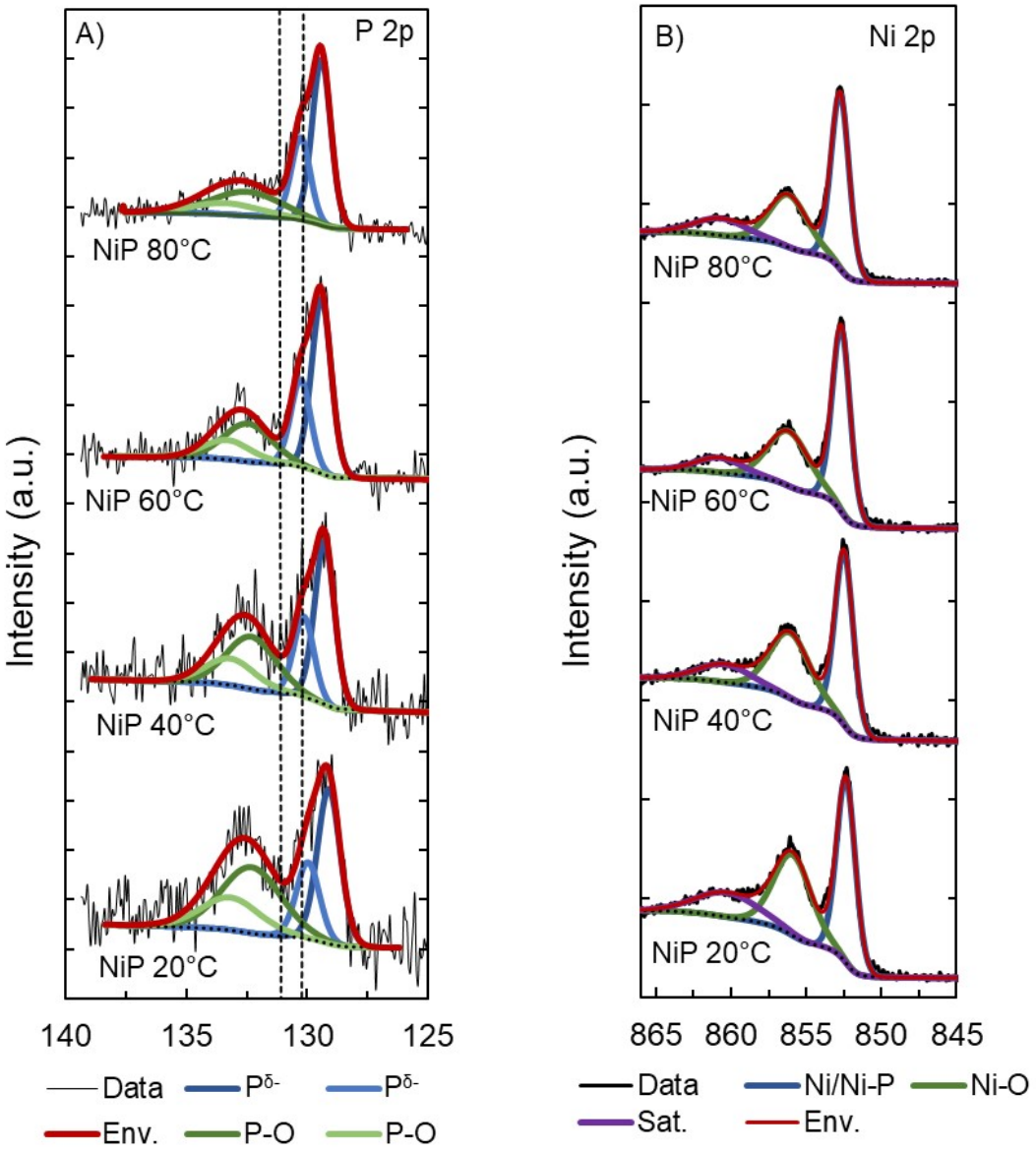

Figure S7. XP spectra of the A) P 2p and B) Ni 2p orbitals of the range of Ni-P films. Dashed vertical lines in A) indicate literature values for the position of the 2p doublet for elemental P.

The peaks in Figure S7 were fit utilizing a Shirley background, with the C 1s peak calibrated to 284.8 eV. The P 2p peaks in Figure S7a were fit as doublets with a separation of 0.86 eV, a relative peak area ratio $2p_{3/2}$: $2p_{1/2}$ of 2:1, and the same FWHM within a doublet. The position of the P $2p_{3/2}$ peak was 129.1 eV, 129.3 eV, 129.4 eV, and 129.4 eV for $NiP_{20°C}$, $NiP_{40°C}$, $NiP_{60°C}$, and $NiP_{80°C}$, respectively. The literature value for the P $2p_{3/2}$ peak of elemental P is 130.2 eV,

meaning that the peak position of P $2p_{3/2}$ in the Ni-P films was shifted by ~ 1 eV. Such a substantial shift in peak position is indicative of a partial negative charge on the P species, which is consistent with the formation of Ni-P bonds. The peak area ratio of the $P^{\delta-}$ (Ni-P) to P-O signals is shown in Table S2. The Ni 2p spectra showed a prominent peak at ~852.5 eV, which is consistent with both the presence of metallic Ni and Ni-P. The complete deconvolution of the Ni 2p spectra, as is the case with any transition metal, is complicated by the amount of Ni multiplet-splitting, a range of stable oxidation states, the presence of multiple nickel oxides, and the presence of shake-up peaks. Additionally, the Ni signal will not be affected by the introduction of P as substantially as the P signal is affected by the Ni, due the low fraction of P in these Ni-P films. However, the decrease of the Ni-O peak relative to the Ni/Ni-P peak is readily quantifiable and is also shown in Table S2.

Table S2. Areal Ratio of Ni and P Signals to Surface Oxide Signals

Deposition Temperature (°C)	$P^{\delta-}$: P-O	Ni+NiP : Ni-O
20	0.9	1.2
40	1.2	1.2
60	1.9	1.5
80	1.9	1.6

For both the P 2p and Ni 2p spectra, the presence of P or Ni oxides, respectively, decreased as the deposition temperature increased. This monotonic decrease in the presence of surface oxides is directly evident by comparing the size of the oxide peaks in Figure S7a and b to the $P^{\delta-}$ and Ni/Ni-P peaks, respectively. As is the case with other surface oxides, these oxides may have formed after the electrodeposition step, when the electrodes were exposed to atmospheric ambient conditions. More reactive surfaces are more susceptible to surface oxidation, so the surface reactivity that results in surface oxidation may be the same instability that results in the eventual cracking of films deposited at low temperatures.

Measuring Transmission and Void Fraction on FTO and n^+-Si substrates

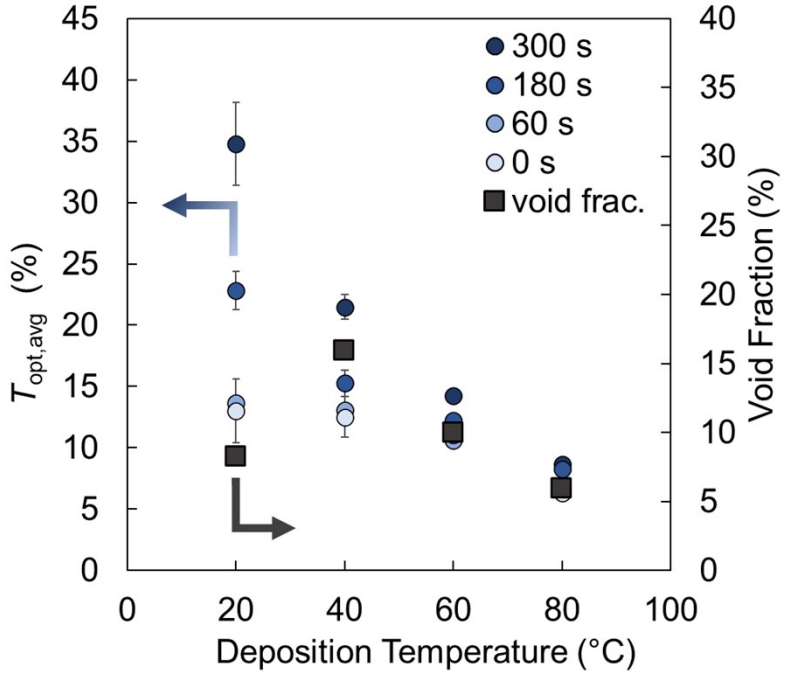

Figure S8. $T_{opt,avg}$ of Ni-P films on FTO substrates compared to the void fraction after immersion in 0.5 M H_2SO_4 for 0 s, 60 s, 180 s, and 300 s determined utilizing a Cary 5000 UV-Vis with an integrating sphere ($T_{opt,avg}$, left) and a FEI Nova NanoSEM 450 (void fraction, right).

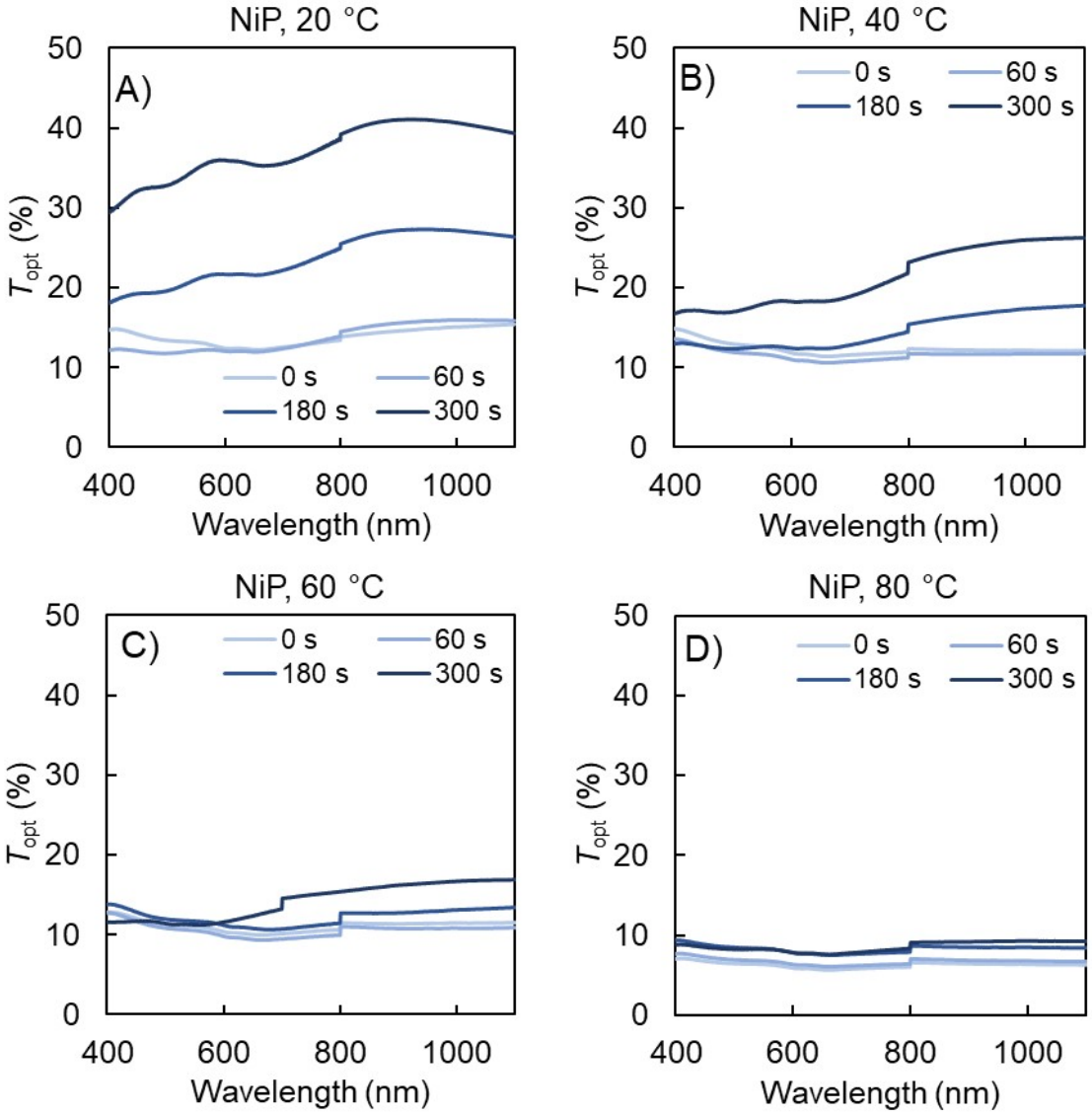

Figure S9. $T_{opt,avg}$ vs. wavelength for selected samples as a function of etch time in 0.5 M H_2SO_4

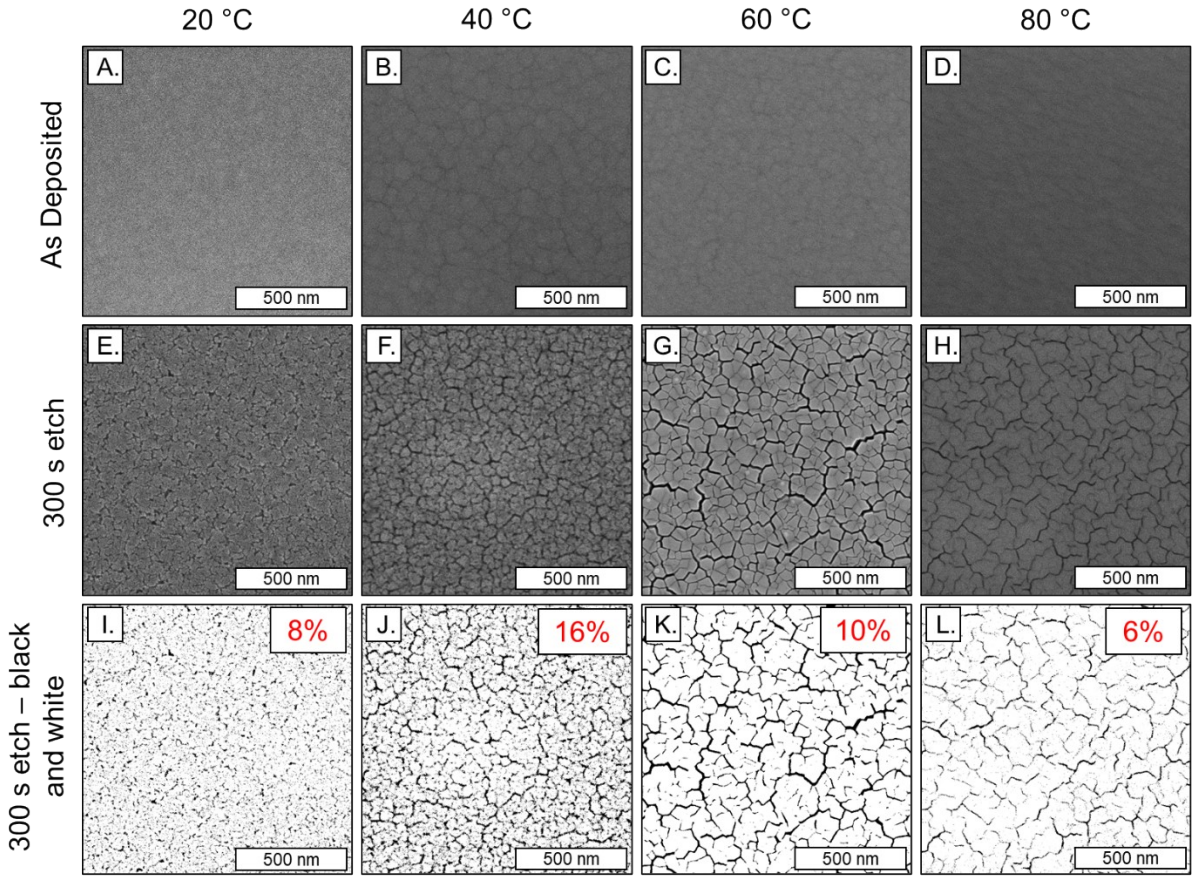

Figure S10. SEMs of NiP films (A-D) as-deposited from 20°C to 80°C; (E-H) after etching for 300 s in 1.0 M H_2SO_4(aq); and (I-L) the same images as (E-H), converted to a black-white 8-bit image to approximate the void fraction. Estimates for the void fraction are shown in red.

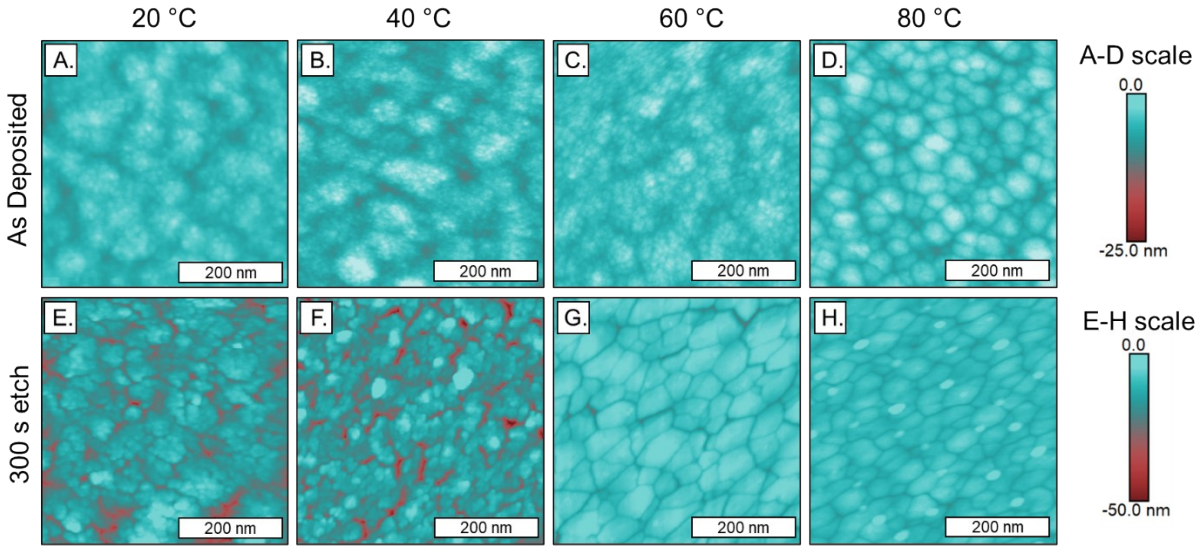

Figure S11. AFMs of NiP films (A-D) as-deposited from 20 °C to 80 °C; (E-H) after etching for 300 s in 1.0 M H_2SO_4(aq).

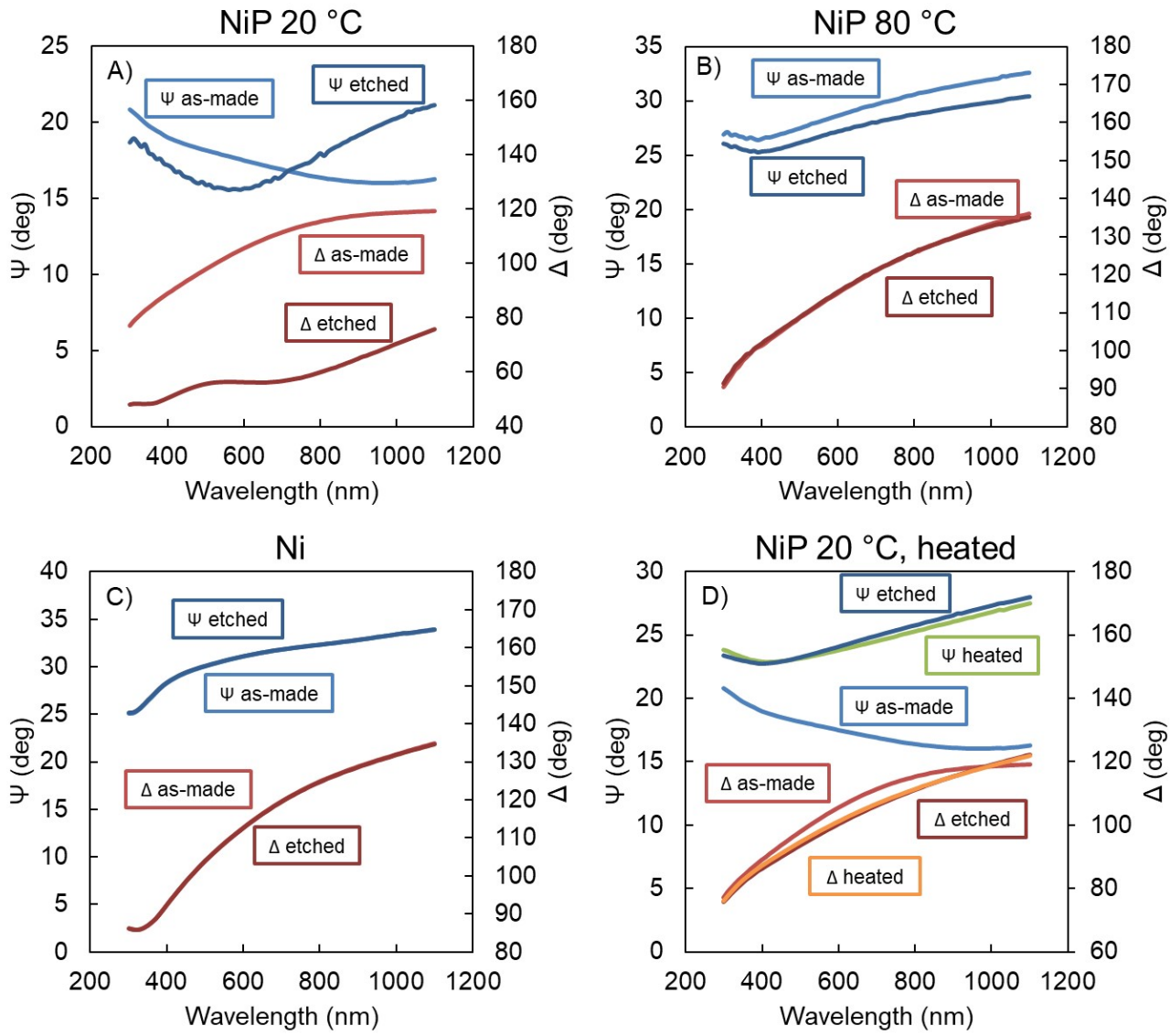

Figure S12. Ψ and Δ measured by spectroscopic ellipsometry of as-made (Ψ light blue, Δ light red) or etched (Ψ dark blue, Δ dark red) films of (a) $NiP_{20°C}$ (b) $NiP_{80°C}$ and (c) sputtered Ni. Ψ and Δ in panel (c) overlapped very closely, and thus the data for the "as-made" films are obscured by the data for the "etched" films. (d) $NiP_{20°C}$ heated to 250 °C in air, displayed with the same color scheme for as-made and etched samples shown in a)-c). The intermediate stage of samples that had been heated without etching is plotted in green (Ψ) and orange (Δ).

Table S3. Activity Summary of Electrodeposited Nickel Phosphide Catalysts

Catalyst Name	Electrodeposition Precursors	Electrolyte	Overpotential at 10 mA cm^{-2}	Reference
Ni_2P Nanosheets	$Ni(NO_3)_2 \cdot 6H_2O$, NaH_2PO_2 phosphidation	0.5 M H_2SO_4	75 mV	Ref.[1]
$Ni_{78}P_{22}$ Films	$NiCl_2 \cdot 6H_2O$, $NaH_2PO_2 \cdot H_2O$	0.5 M H_2SO_4	105 mV	Ref.[2]
Ni/NiP Nanospheres	$NiSO_4$, NaH_2PO_2	0.5 M H_2SO_4	164 mV	Ref.[3]
Amorphous Ni-P (Brenner)	$NiCl_2 \cdot 6H_2O$, NaH_2PO_2, NH_4Cl, $Na_3C_6H_5O_7 \bullet 2H_2O$, NH_4OH	0.5 M H_2SO_4	222 mV	Ref.[4]
Amorphous Ni-P (Acidic)	$NiSO_4 \cdot 6H_2O$, NaH_2PO_2, H_3BO_3, NH_4Cl	0.5 M H_2SO_4	177 mV	Ref.[4]
Ni_5P_4 copper foam nanostructures	$NiCl2 \cdot 6H_2O$, $NaH_2PO_2 \cdot H_2O$, NaH_2PO_4	0.5 M H_2SO_4	90 mV	Ref.[5]
Ni-P/copper foam/carbon paper	$NiSO_4 \cdot 6H_2O$, $NaH_2PO_2 \cdot H_2O$ $C_6H_5Na_3O_7$	0.5 M H_2SO_4	126 mV	Ref.[6]
$Ni_2P/Ni_{12}P_5$	$NiSO_4 \cdot 6H_2O$, $NiCl_2 \cdot 6H_2O$, H_3PO_4, H_3PO_3, NaOH	0.5 M H_2SO_4	170 mV	Ref.[7]
Transparent Co-P Films	$CoCl_2$, $NaPO_2H_2$	0.5 M H_2SO_4	180 mV	Ref.[8]
Transparent Ni-P Films	$NiCl_2$, $H_2NaPO_2 \cdot H_2O$, H_3BO_3, NaCl	0.5 M H_2SO_4	200 mV	This work

Supporting References

1. Cai, Z.-x.; Song, X.-h.; Wang, Y.-r.; Chen, X., Electrodeposition-Assisted Synthesis of Ni2P Nanosheets on 3D Graphene/Ni Foam Electrode and Its Performance for Electrocatalytic Hydrogen Production. *ChemElectroChem* **2015,** *2* (11), 1665-1671.
2. Kim, H.; Park, H.; Kim, D.-K.; Choi, I.; Kim, S.-K., Pulse-electrodeposited nickel phosphide for high-performance proton exchange membrane water electrolysis. *Journal of Alloys and Compounds* **2019,** *785*, 296-304.
3. Ren, Q.; Jin, H.; Xu, X.; Liu, A.; Li, J.; Wang, J.; Wang, S., Hydrogen evolution reaction catalyzed by nickel/nickel phosphide nanospheres synthesized through electrochemical methods. *Electrochim. Acta* **2019,** *298*, 229-236.
4. Wasalathanthri, R. N.; Jeffrey, S.; Su, N.; Sun, K.; Giolando, D. M., Stoichiometric Control of Electrocatalytic Amorphous Nickel Phosphide to Increase Hydrogen Evolution Reaction Activity and Stability in Acidic Medium. *ChemistrySelect* **2017,** *2* (26), 8020-8027.
5. Das, M.; Jena, N.; Purkait, T.; Kamboj, N.; De Sarkar, A.; Dey, R. S., Single-phase Ni5P4–copper foam superhydrophilic and aerophobic core–shell nanostructures for efficient hydrogen evolution reaction. *J. Mater. Chem. A* **2019,** *7* (41), 23989-23999.
6. Yeon, K.; Kim, J.; Kim, H.; Guo, W.; Han, G. H.; Hong, S.; Ahn, S. H., Electrodeposited nickel phosphide supported by copper foam for proton exchange membrane water electrolyzer. *Korean Journal of Chemical Engineering* **2020,** *37* (8), 1379-1386.
7. Bernasconi, R.; Khalil, M. I.; Cakmakci, D. S.; Bektas, Y.; Nobili, L.; Magagnin, L.; Lenardi, C., Electrocatalytic layers for hydrogen evolution reaction based on nickel phosphides: cost-effective fabrication and XPS characterization. *Journal of Materials Science* **2022,** *57* (20), 9370-9388.
8. Kempler, P. A.; Fu, H. J.; Ifkovits, Z. P.; Papadantonakis, K. M.; Lewis, N. S., Spontaneous Formation of >90% Optically Transmissive, Electrochemically Active CoP Films for Photoelectrochemical Hydrogen Evolution. *J Phys Chem Lett* **2020,** *11* (1), 14-20.